Geochemical Perspectives Letters

Potential of Earth's core as a reservoir for noble gases: Case for helium and neon

M.A. Bouhifd, A.P. Jephcoat, D. Porcelli, S.P. Kelley, B. Marty

Supplementary Information

The Supplementary Information includes:

- Starting Materials
- Experimental Techniques
  - Laser Heated Diamond Anvil Cell (LHDAC)
  - Chemical analyses of the run-products
  - Neon in silicate liquids and Fe-rich alloy melts
  - Metal-silicate partition of (He/Ne) ratio
- Table S-1
- Figures S-1 to S-9
- Supplementary Information References

Starting Materials

The CI-model composition (SiO_2 49.6 wt. %, MgO 35.1 wt. %, FeO 8.5 wt. %, Al_2O_3 3.5 wt. %, CaO 3.3 wt. %) is the same starting material used in our previous studies (Bouhifd and Jephcoat, 2006; Bouhifd *et al.*, 2013). The proportions of SiO_2, Al_2O_3, MgO and CaO were chosen to be that of model

CI-chondrite. The mix of CI-chondrite with an FeNi-alloy consisted of 66 wt. % of CI-maj, 24 wt. % Fe metal and 10 wt. % Ni metal. Some experiments were performed using only metallic phase consisting on pure Fe (High purity 99.99+%) or FeNiCo (54 wt. % Fe, 29 wt. % Ni, 17 wt. % Co) metal foils that were obtained from "Goodfellow Cambridge Ltd".

Experimental Techniques

Laser Heated Diamond Anvil Cell (LHDAC)

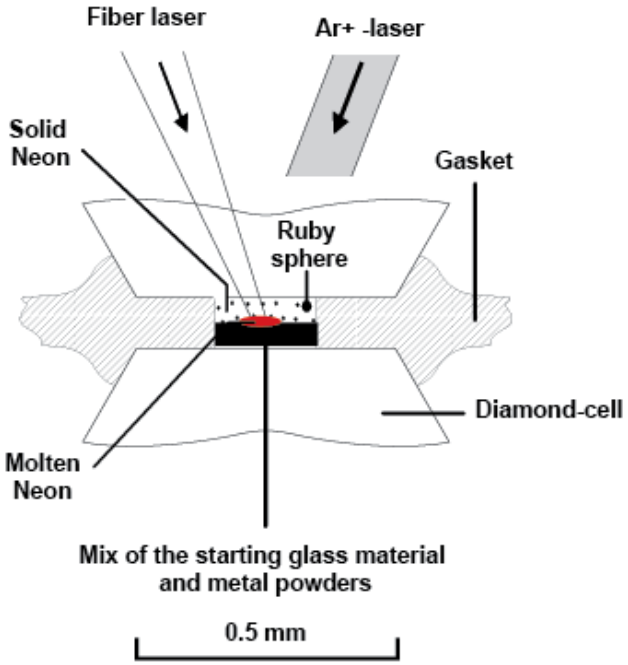

Figure S-1. A typical sample configuration in the Laser Heated Diamond Anvil Cell (LHDAC) for noble gases partitioning experiments (see text for details). Prior to experiments, neon was loaded into the pressure chamber with a high-pressure gas-loading technique at 200 MPa.

For the present experiments we used a set-up similar to that described in previous studies (*e.g.* Jephcoat *et al.*, 2008). We used diamond anvils with 500 µm culets, and stainless-steel gaskets pre-indented to a thickness of ~50 µm and drilled to a diameter of ~100 µm. Samples were mounted in the pressure chamber and neon was loaded with a high-pressure gas-loading technique at 200 MPa. Neon served as pressure-transmitting medium for all runs. The samples were heated by a 100 W air-cooled fibre laser with emission centred at 1070 nm (Model R4, SPI Lasers UK Ltd.) for an average of about 10 to 15 minutes of each zone of the sample (Fig. S-1). To reduce the temperature gradient across the samples, a relatively broad, defocused beam (hot-spot size around 20 microns) was used. With this

temperature gradient, the maximum difference between the temperature at the centre and the edge of the laser spot is 200 degrees (which was taken as a conservative uncertainty on the temperature). Temperatures were determined spectro-radiometrically with a fit to a grey-body Planck function. Great care was taken to scan the hot spot slowly over the whole sample, allowing each part of the sample to be heated to the maximum temperature forming uniform melt pools (either silicate or metal). When the laser beam was initially focused on the starting material, the power was increased slowly until the sample was clearly melted. Several criteria can attest of the melting of the samples at high pressure (*e.g.* Chamorro-Perez *et al.*, 1996), and among these criteria the temperatures of our runs were higher by at least 200 degrees in comparison to the liquidus temperature of peridotite with similar chemical composition to our starting material (*e.g.*, Zhang and Herzberg, 1994; and Fig. S-2).

Finally, during the heating stage the surrounding solid neon, that acts as a pressure-transmitting medium, melted by conductive heating from the heated sample, allowing dissolution of Ne into the sample studied, consistent with the melting curve of neon at high pressure (Santamaria-Pérez *et al.*, 2010). Pressures were measured using the ruby fluorescence method and the hydrostatic pressure scale. For each run, the fluorescence emission of one ruby grain at the edge of the gasket hole was systematically recorded at room temperature before and after heating. We did not observe any difference, within an uncertainty of 10 %, between both pressures. However, in our configuration, an increase of a few GPa on top of the nominal pressures can be expected as deduced from similar LHDAC studies (*e.g.* Andrault *et al.*, 1998). The thermal pressure can be estimated by the following equation: $P_{Th} = \alpha K \Delta T$, where α and K are the thermal expansion and bulk modulus, respectively, and ΔT is the difference between run and room temperatures, respectively. By assuming $\alpha \sim 10^{-5}$, and using the 3rd order Birch-Murnaghan equation of state (with K_0 = 26 GPa and K'_0 = 7 as reported by Guillot and Sator (2007) for a similar silicate melt composition), the pressure correction in our experiments at 5 GPa is about 0.6 and 0.8 GPa at 2500 and 3000 K, respectively. The pressure correction at 14 GPa is about 1.5 GPa between 2500 and 3000 K.

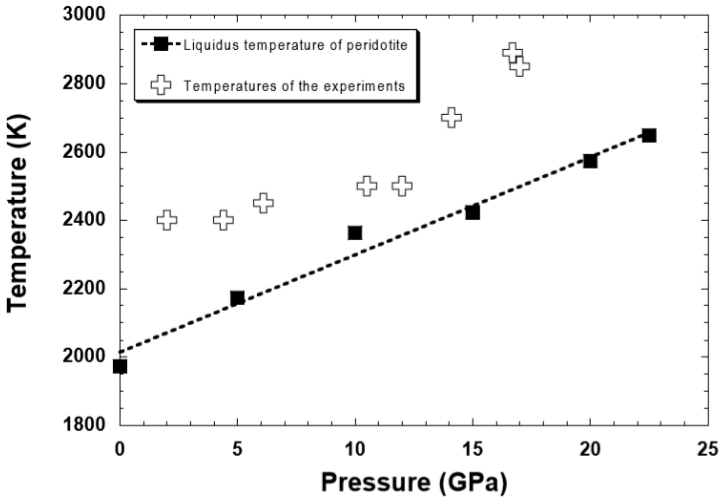

Figure S-2 Temperatures of the experiments in the present study in comparison to the melting temperature of peridotite up to 23 GPa (Zhang and Herzberg, 1994).

Because our experiments are not routine ones the success of our LHDAC technique was demonstrated in our previous studies where we found an excellent agreement between our results and those provided from large volume presses for other volatile elements such as argon (Figs. S-3a – S-3b).

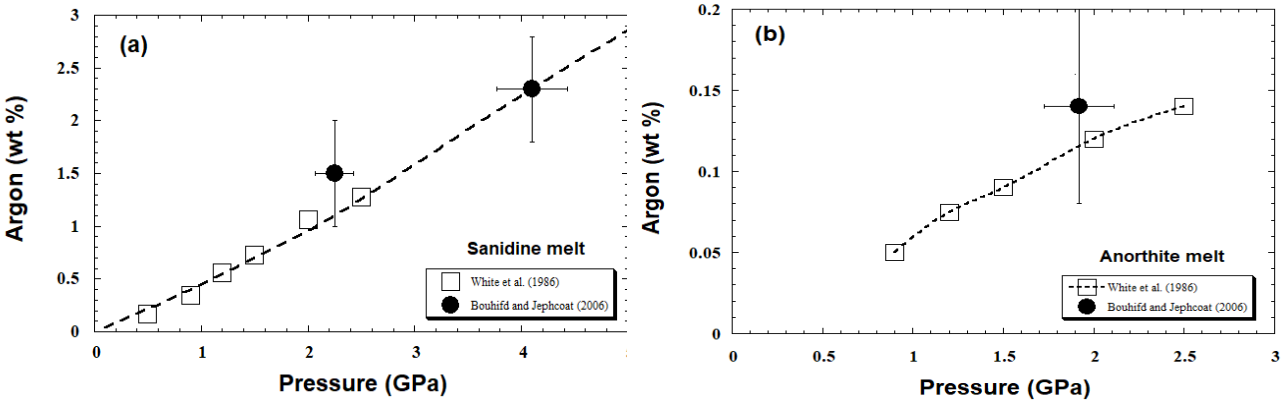

Figure S-3 Ar contents as a function of pressure **(a)** for sanidine melt and **(b)** for anorthite melt. The data from Bouhifd and Jephcoat (2006) are obtained using LHDAC and those of White *et al*. (1986) by using a piston-cylinder apparatus.

Chemical analyses of the Run-Products

Prior to noble gases analyses, the chemical compositions of the run products were analysed by an electron microprobe (JEOL JXA-8800R with 4 wavelength-dispersive spectrometers) with an accelerating voltage of 15 kV and a beam current of 20 nA. Counting times for analyses were about 100s for each analysis. Fe, FeS, Ni and Co metals, orthoclase, jadeite, wollastonite, periclase and corundum were employed as standards.

Table S-1. Chemical composition of the run-products (wt. %). For all our run products we found that the silicate composition is not varying at the present experimental conditions.

Oxides	
SiO_2	47.9 ± 1.2
Al_2O_3	6.2 ± 0.4
FeO	7.1 ± 1.0
MgO	35.5 ± 1.0
CaO	2.8 ± 0.3
Total	**99.5**

Neon analyses in silicate liquids

To determine the partition coefficients of Ne between molten silicate and metal liquid, we consider only the interior bulk concentrations and that we assume to be the equilibrium concentration. So, prior to determine Ne profiles for both phases, we removed the 2 first microns to avoid any high Ne concentrations within the first micrometre depth for both silicate and metal phases. Such high noble gases concentrations near the surface were also observed during our He metal-silicate partitioning study. Note that including the high concentrations near the surface in both silicate and metal leads to similar partition coefficients to those that exclude the surface layer (Bouhifd *et al.*, 2013).

All Ne concentrations results presented here represent at least 1 depth profile (with at least 5 individual and up to 20 Ne analyses). The uncertainties on the reported averaged values (1σ) (see Table 1 in the main text) range from 5 to 20 %.

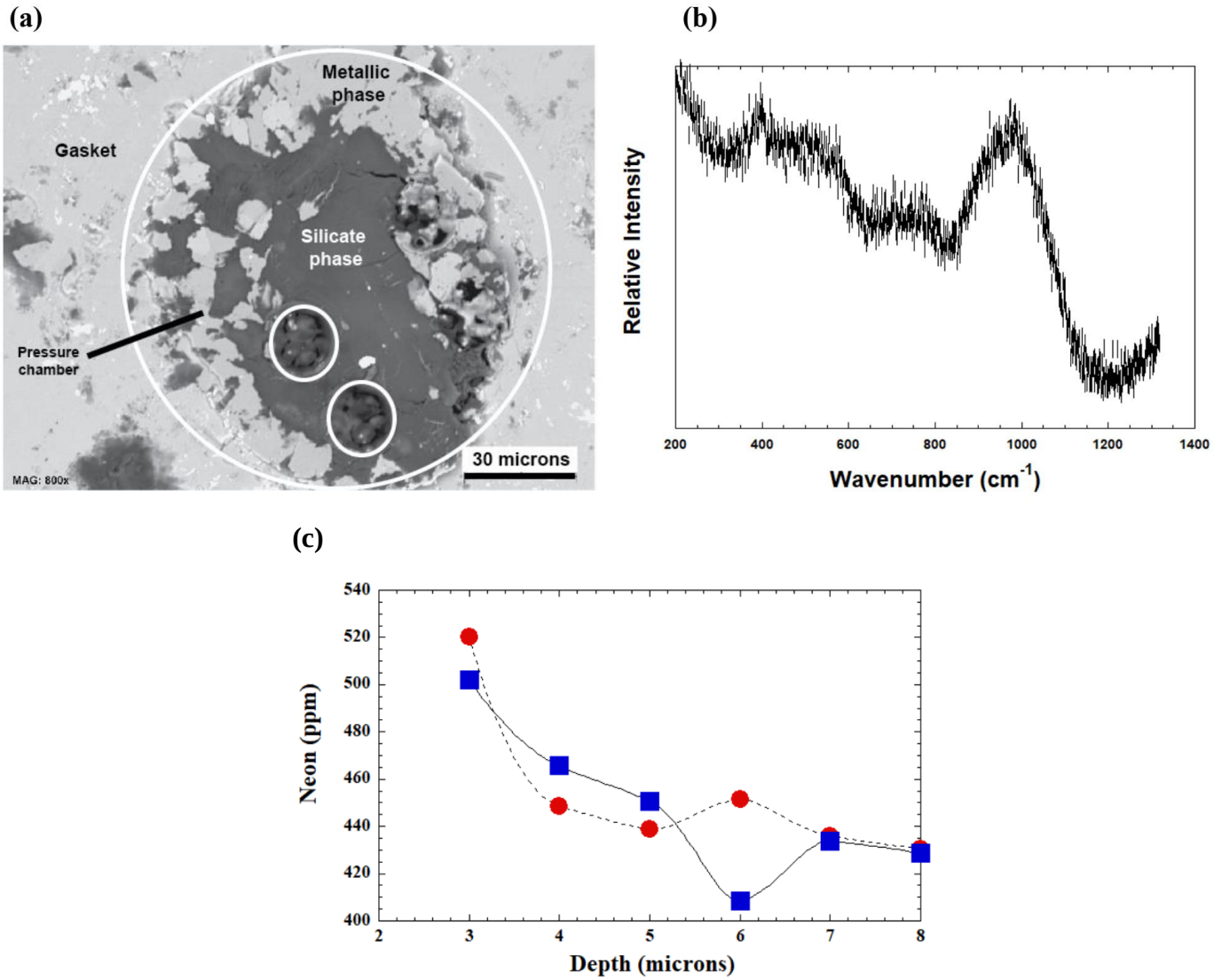

Figure S-4 (a) Back-scattered electron image of run-product quenched from 6.1 GPa and 2500 K. Neon analyses were performed in zones showing a glassy phase formed from quenching the silicate melt from HP. The small white circles show the pits of the laser ablation. **(b)** Raman spectra recorded in zones (glass quenched from HP-HT) prior to neon analyses. **(c)** Depth profiles of Ne concentrations in the silicate phase. Uncertainties are smaller than the symbol sizes (better than 1%) and all data were corrected from the blanks. Lines between symbols serve as a guide only. The two different symbols correspond to different depth profiles within the same run-product reported in Figure S-4a. The average Ne concentration in this sample (6.1 GPa, 2500 K), determined from12 single analyses of 2 profiles, is 451 ± 32 ppm.

For the highest pressures (10 to 16 GPa) of the present work, the Raman study prior to Ne analyses show several features. In the Figure S-5a-b we report a run-product (pure silicate phase) quenched from 10.5 GPa and 2500 K.

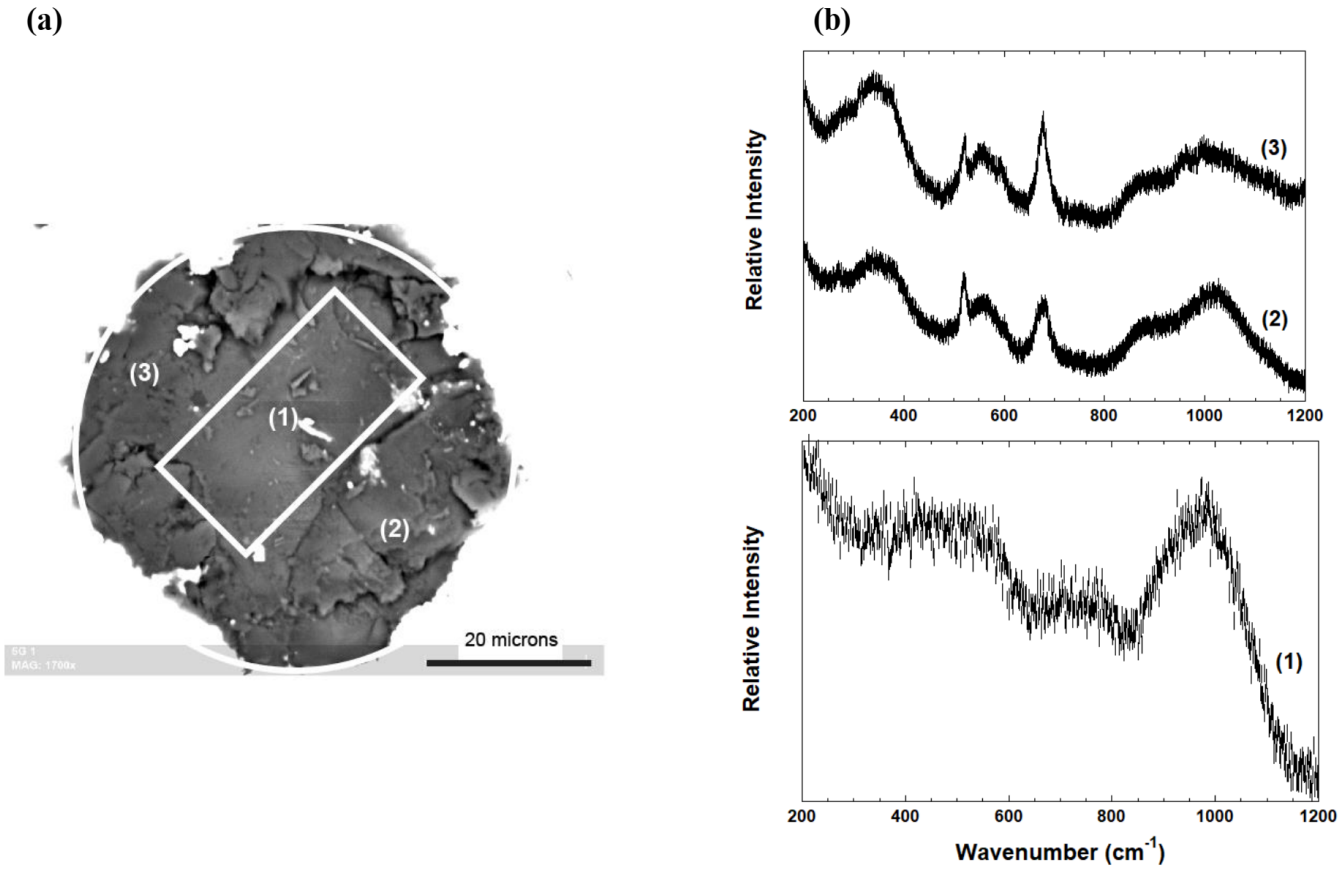

Figure S-5. **(a)** Run-product quenched from 10.5 GPa and 2500 K. Three distinct zones were found in this sample as shown by their respective Raman spectra **(b)**. Zone (1) is a glassy phase, zone (2) is a mix between glass and crystalline phase and zone (3) is a mix between glass and crystalline phases with higher proportion of crystals.

We performed 4 neon profiles on this run-product (2 in zone (1), 1 in zone (2) and 1 in zone (3)) (Fig. S-6). The averaged neon concentrations in zone (1) is 141±15 ppm, in zone (2) is 132±15 ppm and in zone (3) is 120±12 ppm. In zones (2) and (3) that show some recrystallization, the neon concentrations are lower by about 6% and 15% than the concentration for the glassy zone (1). This behaviour is consistent with the study of Niwa *et al*. (2013) on the Ar solubility in SiO_2 melt under high pressures, where they observed a decrease of about 10% of Ar concentration in sample showing crystallization in comparison to a glass quenched from HP-HT. This behaviour is also consistent with the negligible loss of noble gases from the LHDAC samples during the quench. In fact, the much higher thermal diffusivity in a LHDAC (about 10^{-6} to 10^{-7} m^2/s) in comparison to the noble gases diffusion in silicate melts at HP (about 10^{-10} m^2/s) rules out a potential exsolution of noble gases from the heated samples during quenching.

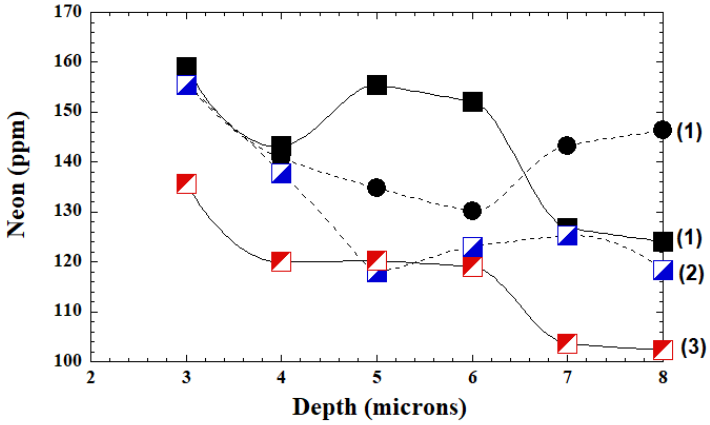

Figure S-6 Depth profiles of Ne concentrations in the silicate phase corresponding to the zones (1), (2) and (3) of the run-product reported in Figure S-5. The partially crystallized zones (2) and (3) contains less Ne by about 6 and 15% in comparison to the glassy zone (1).

Neon in Fe-rich alloy melts

Figure S-7 reports a run-product used to determine Ne concentrations for a molten Fe metal quenched from 8.1 GPa and 2200 K. The two neon profiles show an average neon concentration of 12.1±1.0 ppm.

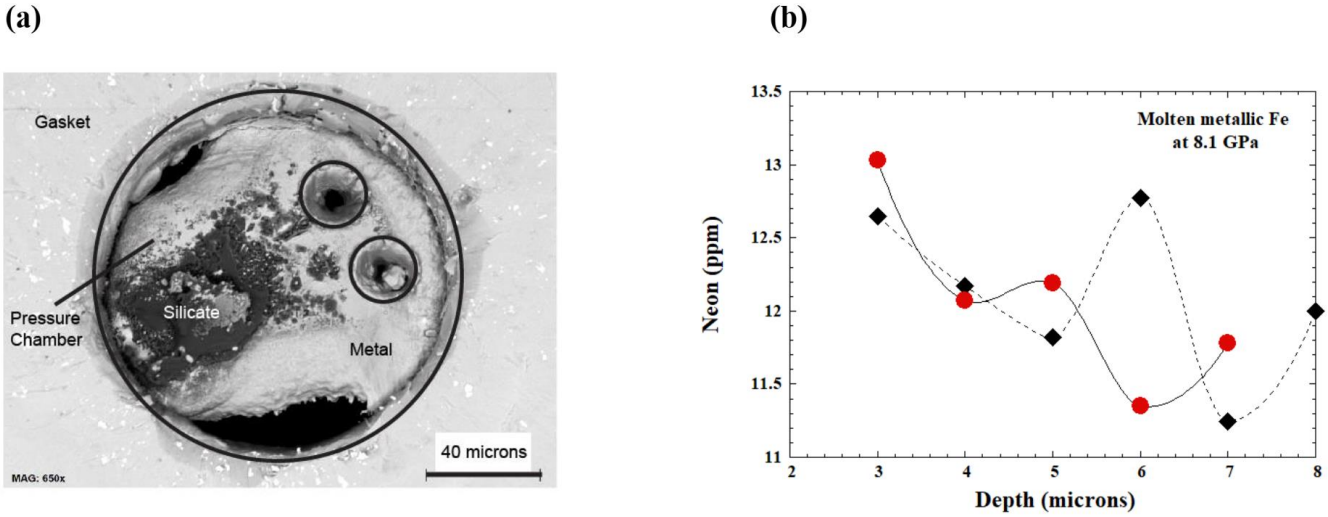

Figure S-7 (a) Back-scattered electron image of run-product analysed for Ne concentrations in metallic Fe. The sample was quenched from 8.1 GPa and 2200 K. **(b)** Depth profiles of Ne concentrations in the metallic phase. The close agreement of the profiles indicates the analytical method is reproducible. Uncertainties are smaller than the symbol sizes (better than 1%) and all data were corrected from the blanks. Lines between symbols serve as a guide only. The different symbols correspond to different depth profiles within the same sample.

Our experiments and analyses show that there is no pressure dependence of neon solubility in Fe-rich alloys, rather it remains relatively constant (within the analytical uncertainties) up to 14 GPa (Figure S-8). All Ne concentrations in metallic phases of this study represent at least 2 depth profiles (with at least 10 individual and up to 20 Ne analyses). The uncertainties on the reported averaged values (1σ) range from 7.5 to 14% (see Table 1 in the main text).

The striking feature here is that we obtain higher concentrations of Ne (13.5±0.8 ppm) in molten Fe-rich alloys in comparison to He concentrations reported in Bouhifd *et al*. (2013). The reason for this behaviour is not understood at this stage but we are planning future experiments where different noble gases will be present simultaneously during metal-silicate partitioning to determine the physical and chemical factors controlling the solubility of noble gases in molten Fe-rich alloys at high pressure.

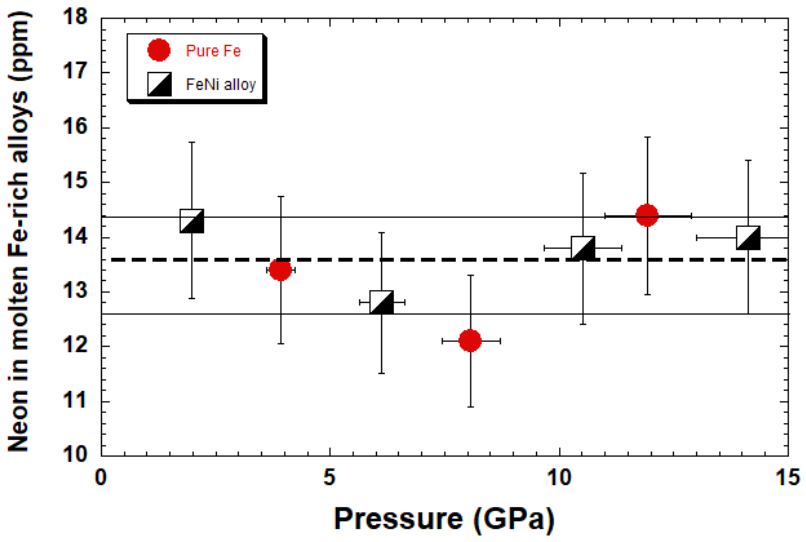

Figure S-8. Neon concentrations in molten metal alloys at high pressures. The reported concentrations are those used to determine the partition coefficients of neon between molten silicate and Fe-rich alloys liquids. We plot constant dashed lines averages of all values of Ne concentrations in metals with the parallel limits representing one standard deviation. The average value for Ne concentrations in molten metal alloys at high pressures is 13.5±0.8 ppm.

Neon and Helium partition coefficients ratio

Combining the metal – silicate partitioning results of Ne and He we observe that $D_{He/Ne}^{metal-Silicate}$ (the ratio of D_{He} over D_{Ne}) is roughly constant and equals to $(5\pm2)\times10^{-2}$. In fact, given the experimental uncertainties, this ratio varies between 2×10^{-2} and 9×10^{-2} (Fig. S-9). In the discussion of our results, we

therefore take D_{He} and D_{Ne} to be within 10^{-3} – 10^{-2} and 10^{-2} – 10^{-1}, respectively, and that $D_{He/Ne}^{metal-Silicate}$ is about 5×10^{-2} during the conditions of Earth accretion and the segregation of its core.

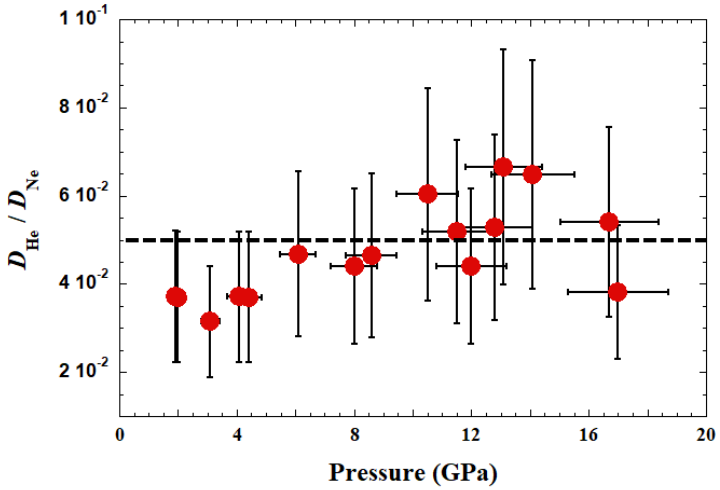

Figure S-9 Metal-silicate partition of (He/Ne) ratio $D_{He/Ne}^{metal-Silicate}$(the ratio of D_{He} over D_{Ne}) versus pressure.

Supplementary Information References

Andrault, D., Fiquet, G., Itié, J.P., Richet, P., Gillet, P., Hausermann, D., Hanfland, M. (1998) Thermal pressure in the laser-heated diamond-anvil cell: an X-ray diffraction study. *European Journal of Mineralogy* 10, 931–940.

Bouhifd, M.A., Jephcoat, A.P. (2006) Aluminium control of argon solubility in silicate melts under pressure. *Nature* 439, 961-964.

Bouhifd, M.A., Jephcoat, A.P., Heber, V.S., Kelley, S.P. (2013) Helium in Earth's early core. *Nature Geoscience* 6, 982-986.

Chamorro-Perez, E., Gillet, P., Jambon, A. (1996) Argon solubility in silicate melts at very high pressures. Experimental set-up and preliminary results for silica and anorthite melts. *Earth and Planetary Science letters* 145, 97-107.

Guillot, B., Sator, N. (2007) A computer simulation of natural silicate melts. Part II: high pressure properties. *Geochimica et Cosmochimica Acta* 71, 4538–4556.

Jephcoat, A.P., Bouhifd, M.A., Porcelli, D. (2008) Partitioning experiments in the laser-heated diamond anvil cell: volatile content in the Earth's core. *Philosophical Transactions Royal Society A* 366, 4295-4314.

Niwa, K., Miyakawa, C., Yagi, T., Matsuda, J. (2013) Argon solubility in SiO_2 melt under high pressures: A new experimental result using laser-heated diamond anvil cell. *Earth and Planetary Science letters* 363, 1-8.

Santamaria-Pérez, D., Mukherjee, D.G., Schwager, B., Boehler, R. (2010) High-pressure melting curve of helium and neon: Deviations from corresponding states theory. *Physical Review B* 81, 214101.

White, B.S., Brearly, M., Montana, A. (1989) Solubility of argon in silicate liquids at high pressures. *American Mineralogist* 74, 513–529.

Zhang, J., Herzberg, C. (1994) Melting experiments on anhydrous peridotite KLB-1 from 5.0 to 22.5 GPa. *Journal of Geophysical Research* 99, 17729-17742.